Scientific Research Publishing

Open Journal of Antennas and Propagation, 2026, 14(2), 23-51
https://www.scirp.org/journal/ojapr
ISSN Online: 2329-8413
ISSN Print: 2329-8421

Wideband Multiresonance Chipless RFID System for Dielectric Crack Detection and Characterization in Structural Health Monitoring Applications

Muzammil Zubair[1*], Fahad Zareen Khan[2], Muhammad Khurram Shahzad[2], Arslan Gul Abbassi[3]

[1]School of Information and Communication Engineering, Northwestern Polytechnical University, Xi'an, China
[2]School of Engineering and Applied Sciences, ISRA University, Islamabad, Pakistan
[3]School of Electrical Engineering, The Arctic University of Norway (UiT), Trondheim, Norway
Email: *muzammilzubair76@gamil.com

How to cite this paper: Zubair, M., Khan, F.Z., Shahzad, M.K. and Abbassi, A.G. (2026) Wideband Multiresonance Chipless RFID System for Dielectric Crack Detection and Characterization in Structural Health Monitoring Applications. *Open Journal of Antennas and Propagation*, **14**, 23-51.
https://doi.org/10.4236/ojapr.2026.142003

Received: June 12, 2026
Accepted: June 27, 2026
Published: June 30, 2026

Abstract

Structural degradation in dielectric materials, particularly cracks and micro-defects, significantly affects the reliability of engineering systems. Conventional non-destructive testing techniques are often limited by cost, intermittent operation, and lack of suitability for continuous monitoring. This paper presents a simulation-based wideband multiresonance chipless RFID sensing framework for quantitative crack estimation in dielectric structures for structural health monitoring applications. The proposed approach introduces a compact LV-shaped resonant tag designed to deliberately engineer multiple stable resonant modes within a wide frequency band, enabling multi-dimensional spectral encoding of structural variations. Unlike conventional single-resonance chipless RFID sensors that primarily support binary detection, the proposed multiresonant configuration enables simultaneous sensitivity to crack width and orientation via independent resonance shifts, thereby enabling quantitative defect characterization. A wideband antipodal Vivaldi antenna is employed as the interrogation unit to ensure efficient excitation and reliable spectral retrieval. Full-wave electromagnetic simulations demonstrate consistent, distinguishable resonance shifts that correspond to variations in crack geometry. The results confirm that the proposed multiresonance chipless RFID system provides a passive, scalable, and simulation-validated framework for multi-parameter crack characterization, enhancing the potential of chipless RFID-based structural health monitoring systems.

Keywords

Wideband Chipless RFID, Multiresonance Sensor, Crack Defect Estimation, Structural Health Monitoring (SHM), Dielectric Materials, LV-Shaped Resonator, Antipodal Vivaldi Antenna, Quantitative Crack Characterization, Passive Wireless Sensing

1. Introduction

Structural health monitoring (SHM) has become a critical requirement for ensuring the safety and reliability of modern infrastructure systems. Compared with conventional nondestructive evaluation (NDE) techniques, SHM enables continuous, distributed monitoring of structural conditions, which is essential for long-term performance assessment of bridges, pipelines, railways, and industrial storage systems. This shift toward real-time condition monitoring has enabled predictive maintenance strategies that reduce both operational risk and lifecycle cost [1]. In high-risk industries such as oil and gas transportation, early detection of structural degradation is essential to prevent catastrophic failures. Defects such as micro-cracks, corrosion, and material fatigue gradually evolve and often remain undetected until structural integrity is severely compromised. In particular, dielectric-based structures used in insulation, coatings, and composite layers are highly vulnerable to crack propagation, which can significantly degrade system performance [2].

Although conventional NDE techniques such as ultrasonic inspection, eddy current testing, and thermography provide accurate defect detection, they are fundamentally limited by their requirement for direct access, high operational cost, and inability to support continuous monitoring over large or inaccessible areas [3]. These limitations motivate the development of autonomous sensing systems capable of wireless, scalable, and long-term operation.

Wireless sensing approaches based on radio-frequency identification (RFID) have emerged as promising alternatives. In particular, chipless RFID systems eliminate the need for integrated circuits by encoding information through electromagnetic resonant signatures. This enables fully passive sensing platforms that are low-cost, lightweight, and suitable for large-area deployment.

However, existing chipless RFID sensing approaches still exhibit critical limitations when applied to structural crack monitoring. Most reported designs rely on single or dual resonant features, which significantly restricts the amount of extractable sensing information. As a result, these systems typically provide only binary or low-resolution defect indication rather than true quantitative characterization.

Furthermore, commonly used resonator types such as dipoles, spirals, and patch-based structures suffer from inherent constraints including limited quality factor stability, polarization dependence, and weak sensitivity to localized dielectric perturbations. Environmental interference, fabrication tolerances, and reader alignment issues further degrade their reliability in practical SHM environments

[4]-[7].

Recent advances have attempted to improve chipless RFID performance through multi-bit spectral encoding and hybrid amplitude-phase techniques. While these methods increase data capacity, they introduce additional system complexity, require precise phase coherence, and remain sensitive to multipath and environmental distortions, limiting their deployment in real-world structural monitoring scenarios [8] [9].

More recently, multi-parameter RFID sensors have been reported for monitoring strain, displacement, and surface defects. Although these approaches demonstrate improved sensing capability, they are generally optimized for metallic substrates and exhibit reduced performance on dielectric materials due to weak field confinement and reduced interaction with localized defects [10]-[15].

To overcome these limitations, this work introduces a wideband, multiresonance, chipless RFID system specifically designed for quantitative crack-defect estimation in dielectric structures. Unlike conventional single-resonance or low-bit encoding tags, the proposed approach employs a compact LV-shaped resonator architecture that supports multiple stable, independent resonant modes across a wide frequency band. These resonances provide enhanced degrees of freedom for capturing subtle variations in crack geometry.

The key innovation of the proposed system lies in its ability to transform crack-induced dielectric perturbations into multi-resonance spectral signatures, enabling not only detection but also estimation of crack width and orientation with improved resolution. In addition, a wideband antipodal Vivaldi antenna is integrated as the interrogation unit, enabling efficient excitation and robust capture of resonance shifts under practical wireless conditions.

Unlike existing chipless RFID SHM systems, the proposed approach enables high-resolution, passive, and scalable crack characterization in dielectric structures, making it suitable for long-term monitoring of critical infrastructure.

2. Multiresonance Chipless RFID Sensor Tag Operation

The proposed sensing architecture is based on a wideband multiresonance chipless RFID tag that encodes structural information directly into its frequency-domain scattering signature, as illustrated in **Figure 1**. Unlike conventional RFID identification schemes that rely on single-resonance or binary spectral encoding, the proposed system exploits multiple independently excited resonant modes to significantly expand the sensing dimensionality for defect characterization. In this framework, the sensor tag operates as a passive electromagnetic transducer, where its scattering response is governed by the interaction between incident electromagnetic waves and the local dielectric environment of the monitored polyamide structure. Any variation in structural integrity, such as crack formation or propagation, perturbs the effective permittivity distribution around the tag, resulting in measurable shifts in multiple resonant frequencies.

The interrogation mechanism is based on a wideband radar-inspired excitation signal transmitted from the reader unit, enabling simultaneous excitation of all resonant modes within the tag. To enhance detection robustness and suppress direct coupling between transmitter and receiver, a cross-polarized configuration is employed. The transmitting antenna radiates a vertically polarized field, while the receiving antenna is oriented orthogonally to capture only the depolarized scattered response, thereby improving signal to clutter isolation in complex environments [16] [17]. Upon excitation, the multiresonance tag exhibits a frequency-selective scattering behavior in which each resonant mode acts as an independent sensing channel. These resonances are not only determined by the geometric configuration of the tag but are also highly sensitive to localized dielectric perturbations induced by structural defects in the underlying material. This enables the conversion of spatial crack variations into a high-dimensional spectral signature. The received backscattered signal is processed in the frequency domain to extract the multiresonant signature of the tag. Changes in resonance frequency spacing, amplitude variation, and spectral distortion collectively provide a richer feature set for quantitative defect estimation, rather than simple binary detection.

Compared to conventional chipless RFID sensing approaches that rely on limited resonance count or single-parameter sensitivity, the proposed multiresonance architecture introduces an enhanced sensing framework capable of capturing higher-order electromagnetic interactions between the tag and the damaged dielectric medium. This results in improved resolution and increased robustness for structural health monitoring applications.

Figure 1 illustrates the operating principle of the proposed chipless RFID sensing system, including wideband interrogation, cross-polarized transmission/reception, and the depolarized backscattered response from the sensor tag.

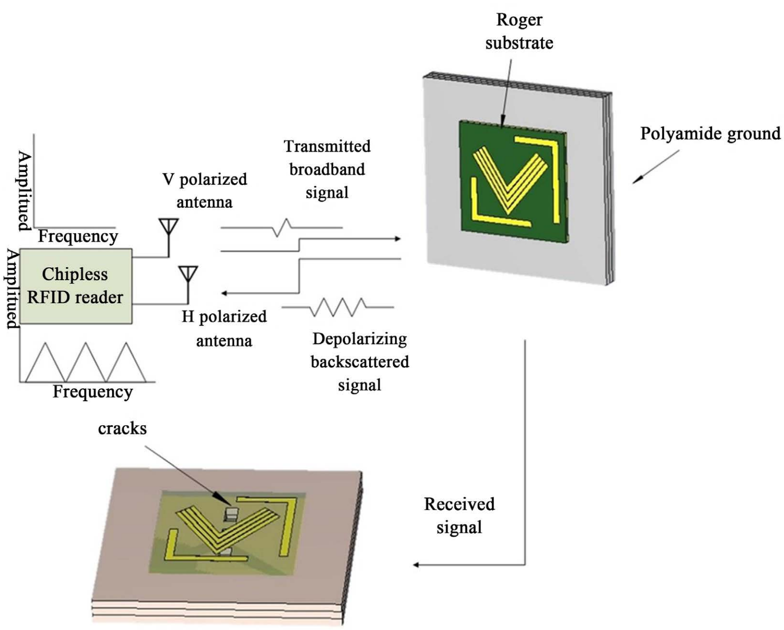

Figure 1. Principle of operation of Chipless RFID sensor.

2.1. Physical Sensing Mechanism

The proposed chipless RFID sensor operates by exploiting the interaction between the resonant electromagnetic fields of the LV-shaped resonator and the dielectric material under inspection. The sensing structure consists of an LV-shaped copper resonator printed on a dielectric substrate backed by a continuous copper ground plane. The resonator generates localized fringing electric fields that extend into the polyamide specimen.

When a crack is introduced into the polyamide, part of the dielectric material is replaced by air, reducing the effective dielectric constant in the sensing region. This dielectric perturbation alters the effective capacitance of the resonator, resulting in measurable shifts in the resonant frequencies. Since the LV-shaped resonator supports multiple resonant modes, each mode exhibits a distinct sensitivity to crack geometry, allowing for the characterization of both crack width and orientation.

2.2. Generation of Multiple Resonance and the Principle of Dielectric Defect Sensing

The proposed chipless RFID sensing tag is based on a multiresonance electromagnetic scattering architecture implemented using a microstrip patch-based configuration. In this system, the conductive patch layer is positioned above a dielectric substrate, while the ground plane is conceptually associated with the monitored polyamide structure. This configuration enables strong near-field electromagnetic interaction between the resonant elements and the host material, thereby converting the conventional patch antenna into a distributed dielectric-sensing transducer.

From an electromagnetic perspective, each microstrip patch operates as a cavity resonator that exhibits frequency-selective scattering behavior. The resonant condition is governed by the effective electrical length of the patch and the equivalent permittivity of the surrounding medium. The fundamental resonant frequency of a rectangular microstrip patch can be expressed as:

$$f_r = \frac{C}{2\sqrt{(L+2\Delta L)}\sqrt{\varepsilon_r}}$$

where f_r is the resonant frequency, C is the speed of light in a vacuum, L is the patch's physical length, ΔL is the fringing extension added to L, and ε_r is the substrate's relative permittivity. Any perturbation in the local electromagnetic environment directly modifies the effective permittivity and boundary conditions of the resonator, resulting in measurable shifts in resonant frequency. These shifts form the fundamental sensing principle of the proposed system, where structural defects are mapped into variations of the multiresonant spectral signature.

To enhance sensing dimensionality, multiple microstrip resonators with distinct geometrical configurations are integrated within a compact sensing region. Each resonator contributes an independent spectral response, enabling the formation of a wideband multiresonance signature. This multi-mode response significantly increases the information content of the backscattered signal, allowing improved resolution for defect characterization.

From a field-theoretical perspective, incident electromagnetic waves induce surface current distributions and charge accumulation across the patch-ground interface. These induced currents act as the primary source of backscattered radiation. When structural discontinuities are present, the current flow paths are disturbed, leading to modified resonance conditions that manifest as frequency shifts, amplitude variations, and spectral distortion.

In the case of dielectric crack defects, the presence of a crack introduces a localized geometrical discontinuity that disrupts current continuity on the effective ground plane region. This disruption creates anisotropic perturbations in the current distribution, meaning that both crack width and orientation influence the degree of resonance shift. As a result, crack characteristics are encoded into the spectral response, enabling quantitative defect estimation rather than simple binary detection.

In contrast, corrosion-related degradation and coating layers introduce distributed changes in the effective electromagnetic medium. The presence of multiple material layers—including base polyamide, corrosion products, and protective coatings forms a complex multilayer dielectric stack. These layers collectively alter the effective permittivity, permeability, thickness, and loss tangent experienced by the resonant modes.

Since electromagnetic field penetration is frequency-dependent, different resonant modes interact with different effective depths of the material stack. This results in mode-dependent resonance perturbations, allowing the system to capture both surface-localized and subsurface material variations.

Therefore, the proposed multiresonance chipless RFID architecture provides a high-dimensional electromagnetic sensing framework, where localized crack defects and distributed corrosion effects are simultaneously mapped into a multiresonant spectral signature. This enables enhanced sensitivity, improved feature richness, and more accurate structural health assessment compared to conventional single-resonance or narrowband chipless RFID sensing systems.

3. Design of LV-Shaped Multiresonance Chipless RFID Sensor Tag

The proposed sensing element is a wideband multiresonance chipless RFID tag based on an integrated L-shaped and V-shaped depolarizing resonator configuration. The LV geometry is specifically engineered to support multiple orthogonal current paths and controlled electromagnetic coupling mechanisms, resulting in enhanced spectral richness for dielectric defect estimation in structural health monitoring applications. The geometrical layout and key design parameters are illustrated in Figure 2. Unlike conventional single-resonance chipless RFID tags, the proposed structure is not designed solely for frequency allocation but for multi-mode electromagnetic scattering generation, where each resonant segment contributes independently to the overall spectral signature. This enables higher information density and improved sensitivity to small variations in the surrounding dielectric environment.

The tag is fabricated on a Rogers RO3035 lossy substrate with dielectric constant $\varepsilon_r = 3.5$ and loss tangent $\delta = 0.0023$. The top metallization layer consists of the LV-shaped copper resonator, while the bottom layer forms a continuous copper ground plane with a thickness of 0.018 mm. The monitored polyamide structure is positioned beneath the ground plane and acts as a lossy sensing medium, enabling direct electromagnetic interaction with the resonant field distribution. The substrate thickness is fixed at $h = 1.52$ mm, and both substrate and ground plane share identical lateral dimensions of 35 × 35 mm. The sensing medium (polyamide structure) is extended to 60 × 60 mm to ensure sufficient field penetration and to minimize edge reflection effects, thereby improving the reliability of dielectric interaction modeling.

The design methodology follows a sensing-driven resonator synthesis approach, where classical microstrip antenna theory is adapted not for radiation optimization but for maximizing dielectric perturbation sensitivity and multiresonance separation. The fundamental electromagnetic behavior is first related to resonant wavelength as:

$$\lambda = \frac{C}{f} \tag{1.1}$$

where C is the velocity of light and f is the resonance frequency. The patch width is then defined using Equation (1.1).

w is the width of the patch, and the relative permittivity of the substrate is ε_r. The effective electromagnetic behavior of the resonator is governed by the interaction between the physical geometry and the surrounding dielectric environment, which is expressed through

$$W = \frac{C}{2f}\sqrt{\frac{2}{\varepsilon_r + 1}} \tag{1.2}$$

$$L_{eff} = \frac{C}{2f\sqrt{\varepsilon_{reff}}} \tag{1.3}$$

where C the speed of light in a vacuum L_{eff} is the effective length of the patch, and ε_{reff} is the substrate's effective relative permittivity L_{eff} takes into account both physical length and fringing fields at the patch's tips, resulting in:

$$L' = L_{eff} + 2\Delta L \tag{1.4}$$

L' is the length of the patch which is equal to the effective length ($L_{eff} + 2\Delta L$), whereas ΔL is the extended length, ΔL can be further elaborated as

$$\Delta L = 0.042h\frac{\left(\varepsilon_{reff} + 0.3\right)\left(\frac{w}{h} + 0.0264\right)}{\left(\varepsilon_{reff} + 0.258\right)\left(\frac{w}{h} + 0.8\right)} \tag{1.5}$$

where w is the patch's width and h is the thickness of the substrate underneath the patch. In both (1.3) and (1.5), ε_{reff} is related to the dielectric constant ε_r, w and h of the substrate, and may therefore be represented as:

$$\varepsilon_{reff} = \frac{\varepsilon_r + 1}{2} + \frac{\varepsilon_r - 1}{2}\left(1 + 12\frac{h}{w}\right)^{-\frac{1}{2}} \tag{1.6}$$

The Equations (1.4) to (1.5) describe the relationships between the resonance of a V-shaped patch and several parameters, including the patch's length and width, substrate thickness, and substrate permittivity. These estimate equations are valid for a V-shape patch constructed on a Roger substrate. Substrate length and width are calculated by using the following formulas, which are given below.

Whereas Lg & Wg are the length and width of the substrate, and h is given by

$$h = \frac{0.0606\lambda}{\sqrt{\varepsilon_r}} \tag{1.7}$$

Figure 2 illustrates the configuration of the LV-shaped chipless RFID sensor and identifies the principal geometrical parameters used to define the resonant structure.

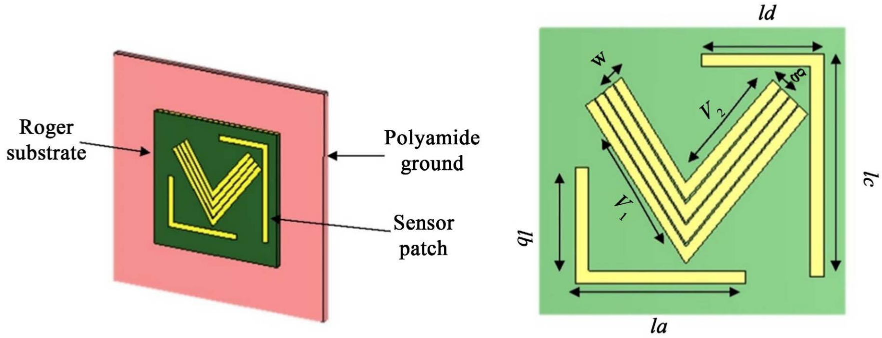

Figure 2. Configuration and geometrical characteristics of a chipless RFID sensor.

The detailed geometrical parameters of the proposed structure are provided in Table 1, which defines the dimensional variations of each resonant arm responsible for multiresonance generation.

Table 1. Dimension of Multiresonance Chipless RFID sensor.

h	*g*	*la*	*lb*	*lc*	*ld*	V_1	V_2	*ta*	*W*
1.52	0.52	29	27	26	16	21	14	0.018	2

4. Simulation of L & V Shape-Based Multiresonance Chipless RFID Sensor Tag

This section established the principle of multiresonance generation for dielectric crack defect estimation using microstrip resonators [16]. Building on this concept, the present study employs a cross-polarized interrogation framework, where the chipless RFID tag operates as a depolarizing electromagnetic scatterer [16] [17]. This enables robust separation of the transmitted and backscattered signals, improving detection reliability in practical structural health monitoring environments.

The proposed design is inspired by the concept of radio-frequency encoding particles [18], where multiple resonant scattering elements are engineered to encode information in the frequency domain. In this work, the concept is extended by integrating L-shaped and V-shaped resonant geometries into a unified LV-shaped architecture to achieve enhanced multiresonance behavior and improved dielectric sensitivity.

The final configuration of the proposed chipless RFID sensor tag is illustrated in **Figure 3**. The structure consists of a combination of diagonal dipole-based resonators arranged in L and V geometries with varying physical lengths. The V-shaped section is formed by two orthogonal sets of dipole arms: one set al.igned diagonally and the other oriented orthogonally, resulting in controlled current redistribution and strong depolarization effects [16] [17]. Two additional L-shaped resonators are positioned adjacent to the V-shaped structure to further enhance multiresonance generation and spectral diversity.

From an electromagnetic perspective, this hybrid arrangement induces multiple current paths and coupling mechanisms within a compact footprint, leading to the formation of distinct resonant modes across the operating bandwidth. These resonances collectively form a wideband multiresonance spectral signature, which is highly sensitive to variations in the surrounding dielectric environment [18].

Each resonant element is etched on a Rogers RO-3035 substrate with a relative permittivity of 3.5 and a thickness of 1.52 mm. The total footprint of the sensor tag is maintained at 35 mm × 35 mm to ensure compact integration while preserving sufficient field confinement for stable resonance behavior. The monitored polyamide structure lies beneath the ground plane and interacts with the fringing electromagnetic fields, enabling defect-induced perturbations in the scattering response [19].

The proposed LV configuration is specifically designed to enhance mode diversity, polarization conversion efficiency, and resonance separation, which are critical factors for improving crack defect estimation accuracy [16]-[18]. Unlike conventional single-geometry chipless RFID tags, the hybrid LV structure introduces controlled asymmetry and orthogonal coupling paths, resulting in richer spectral encoding capability.

Figure 3 illustrates the full-wave simulation setup used to evaluate the multiresonance RCS response of the proposed chipless RFID sensor under plane-wave excitation.

4.1. Simulation Methodology

The proposed chipless RFID sensor was modeled and analyzed using CST Studio Suite over the 2 - 6 GHz frequency range. Simulations were performed using the

Frequency Domain/Time Domain solver with Open (Add Space) boundary conditions. An adaptive mesh refinement was employed until the predefined convergence criterion was satisfied.

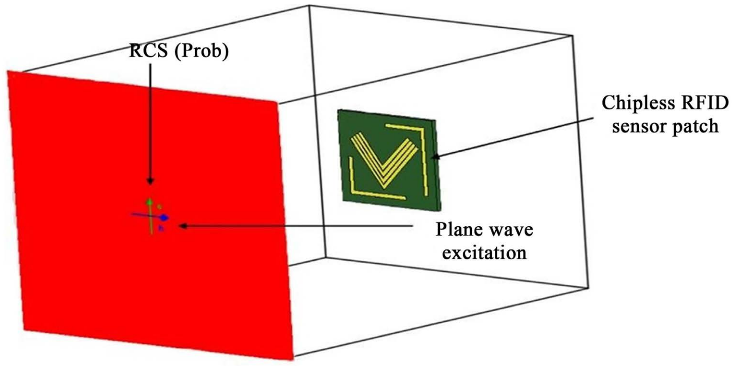

Figure 3. Simulation setup of the multiresonance chipless RFID sensor.

The sensing structure consists of an LV-shaped copper resonator backed by a continuous copper ground plane. The inspected material was modeled as polyamide with a relative permittivity of $\varepsilon r = 3.5$ and a loss tangent of $\tan\delta = 0.005$. Crack widths of 1 - 3 mm with orientations of 0˚, 45˚, 90˚, and 135˚ were simulated to evaluate their effects on the resonant response. All other simulation parameters were kept constant throughout the study.

4.2. Substrate Optimization and Multiresonance Radar Cross-Section Characteristics

The selection of substrate relative permittivity and thickness plays a critical role in determining the electromagnetic scattering performance of the proposed wideband multiresonance chipless RFID sensor tag. In particular, these parameters are optimized to enhance the radar cross-section (RCS), which directly governs the detectability of the tag under cross-polarized interrogation conditions. A higher RCS ensures stronger backscattered signal strength, improving the reliability of tag recognition at the reader side. From a system perspective, the achievable read range is fundamentally governed by the radar range equation, where the tag's RCS acts as a key scattering parameter influencing the received signal power [20].

The substrate permittivity introduces a trade-off between electromagnetic confinement and scattering efficiency. Lower permittivity substrates increase the effective electrical size of the resonant patches, which generally enhances RCS due to stronger scattering. However, this also reduces the quality factor of the resonances, leading to broader spectral peaks and reduced frequency selectivity. Similarly, increasing substrate thickness improves scattering strength and RCS performance but may introduce additional dielectric losses and mode distortion effects if not properly optimized [21].

Established RCS-synthesis and RF-encoding-particle frameworks further support the frequency-domain interpretation of chipless RFID backscatter and resonant coding adopted in this work [22] [23].

Therefore, the substrate parameters are carefully selected to achieve a balanced trade-off between high RCS for reliable detection and sufficient quality factor for distinct multiresonance separation. This balance is essential to ensure that multiple resonant peaks remain distinguishable while maintaining strong backscatter response for practical chipless RFID interrogation. In addition to material selection, the geometry of the LV-shaped resonator is optimized to generate multiple resonant modes within a compact footprint. The spatial configuration and resonator lengths are engineered to ensure adequate separation between resonant frequencies while preserving strong scattering efficiency, enabling simultaneous high detectability and high spectral resolution.

Under the optimized design, the proposed sensor tag exhibits six distinct resonant responses within the 2 - 6 GHz band. The resonant frequencies are observed at 2.29 GHz, 2.73 GHz, 3.11 GHz, 3.74 GHz, 4.51 GHz, and 5.1 GHz, respectively. These well-distributed resonances form a wideband multiresonance spectral signature, which enhances sensitivity to dielectric perturbations and enables improved crack defect estimation capability.

Figure 4 shows the simulated RCS spectrum of the optimized sensor, where six distinct resonant responses are observed across the 2 - 6 GHz operating band.

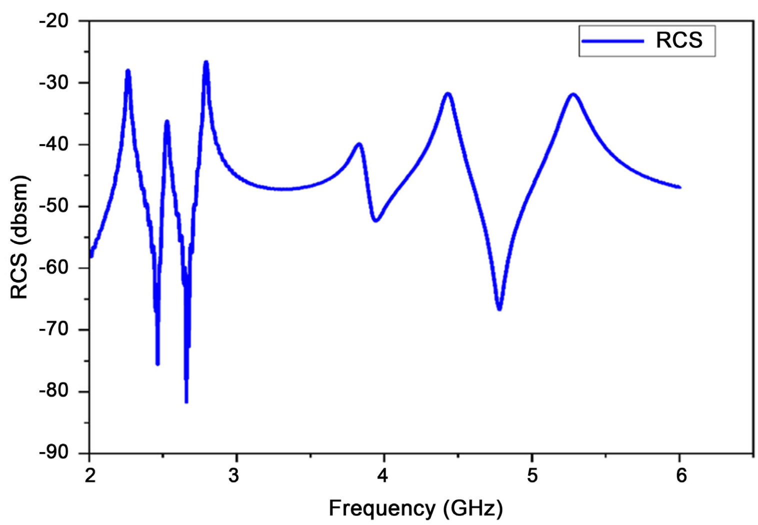

Figure 4. Simulated RCS spectra of the multiresonance chipless RFID sensor.

4.3. Origin of Multiresonance Response and Crack-Dependent Spectral Behavior

To further explain the origin of the six observed resonances, the surface current distributions at the corresponding resonant frequencies are analyzed in **Figure 5(a)**, **Figure 5(b)**. The multiresonance behavior of the proposed wideband chipless RFID sensor is directly governed by the independent excitation of L-shaped and V-shaped resonant paths, each contributing distinct electromagnetic modes within the operating bandwidth.

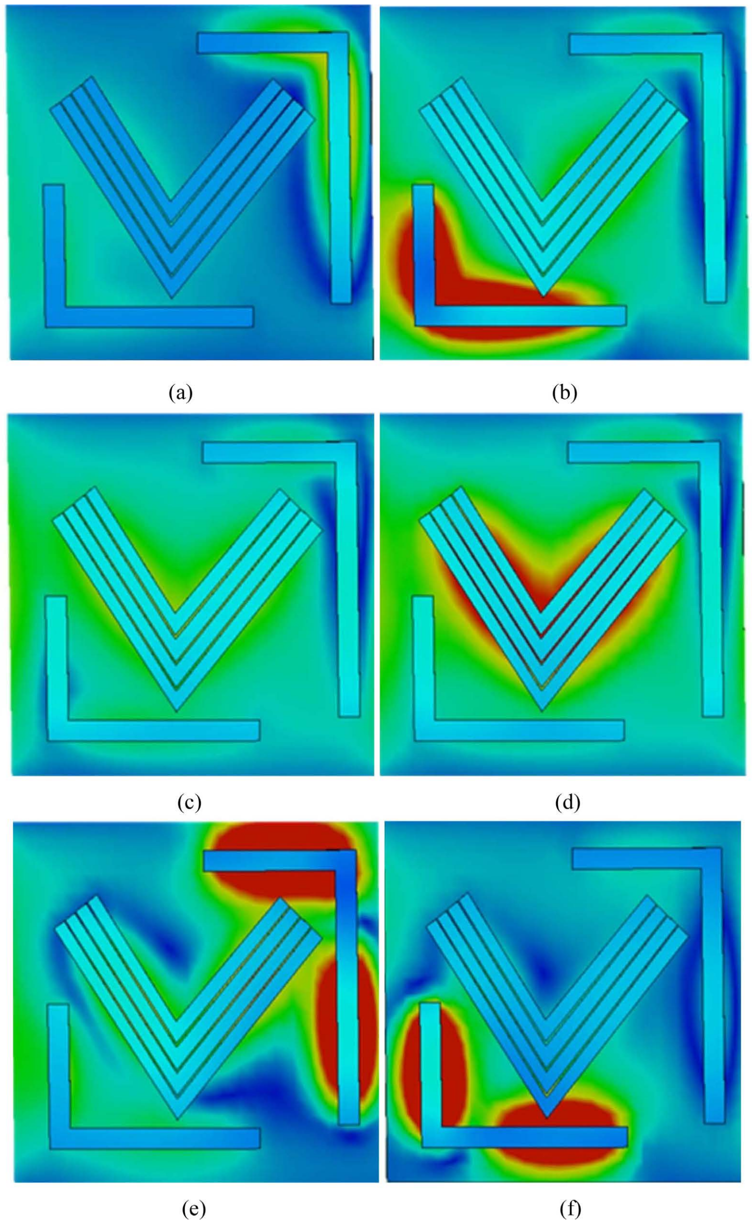

Figure 5. Current distributions at the surface of the multiresonance chipless RFID (a) 2.29 GHz; (b) 2.73; (c) at 4.51 GHz; (d) 4.8 GHz; (e) at 4.51 GHz; (f) 4.8 GHz.

The first two resonant peaks at 2.29 GHz and 2.73 GHz originate from the L-shaped resonators. These resonances are primarily determined by the effective electrical lengths of the L-shaped current paths. Specifically, the longer L-shaped arm exhibits a lower resonant frequency due to increased effective current path length, while the shorter arm supports a higher-frequency resonance. This confirms that the L-shaped geometry operates as a length-dependent resonant scatterer within the multiresonance framework.

The next two resonant modes at 3.11 GHz and 3.74 GHz are generated by the V-shaped resonant configuration. The orthogonal arrangement of the V-shaped dipole arms produces controlled current redistribution and enhanced depolarization behavior, resulting in additional distinct resonant states. These modes are strongly influenced by the angular orientation and coupling between the diagonal dipole segments, which increases spectral diversity within the tag response.

The final two resonances at 4.51 GHz and 5.1 GHz are attributed to higher-order harmonic responses of the L-shaped resonators. These resonances arise due to partial current excitation along segmented portions of the L-shaped geometry, where current distribution becomes non-uniform and supports higher-order resonant modes. As a result, each L-shaped element contributes multiple spectral features rather than a single resonance, significantly increasing the overall information density of the tag.

The defect sensing mechanism becomes evident through the analysis of surface current perturbations. Any structural discontinuity in the underlying polyamide layer modifies the current distribution on the ground interface, leading to changes in both the amplitude and frequency position of the resonant peaks. This perturbation directly translates into variations in the radar cross-section (RCS) response, forming the basis for crack-dependent spectral encoding.

To evaluate crack sensitivity, a parametric study is performed by varying crack width from 0 mm to 3 mm in 1 mm steps, while fixing crack depth at 2 mm. In addition, crack orientation angles of 0˚, 45˚, 90˚, and 135˚ are considered to analyze directional sensitivity. This systematic sweep enables quantitative assessment of how crack geometry influences multiresonance frequency shifts and RCS variations, thereby validating the proposed sensor for crack defect estimation in structural health monitoring applications.

4.4. Simulation Study of Orientation-Dependent Dielectric Crack Detection

To investigate the influence of dielectric cracks on the radar cross-section response of the proposed sensor, cracks with widths of 1, 2, and 3 mm were introduced into the polyamide specimen. Four crack orientations, namely 0˚, 45˚, 90˚, and 135˚, were considered while the remaining geometrical and material parameters were kept unchanged. The resulting RCS spectra were compared with the intact-specimen response.

A dielectric crack locally replaces part of the polyamide with air and therefore changes the effective dielectric loading experienced by the LV-shaped resonator. This perturbation modifies the localized electric-field distribution and electromagnetic coupling between the resonant elements and the monitored specimen. Consequently, variations in crack width and orientation produce changes in the frequency positions and amplitudes of the multiresonance response.

For each resonant mode, the crack-induced frequency variation is defined as

$$\Delta f_{i,\theta}(w) = f_{i,\theta}(w) - f_{i,0}, \tag{1.8}$$

where $f_{i,\theta}(w)$ denotes the frequency of the ith resonance for crack width w

and orientation θ, and $f_{i,0}$ represents the corresponding resonance frequency of the intact specimen. A positive value of Δf indicates a shift toward a higher frequency, whereas a negative value represents a shift toward a lower frequency.

In the proposed sensing framework, crack width is represented by the magnitude of the multiresonance frequency variation, whereas crack orientation is characterized by the distribution and direction of the shifts across the selected resonant modes. Therefore, the complete multiresonance signature, rather than a single resonance, is used to distinguish the investigated crack conditions.

Figure 6 presents the simulated RCS response for the horizontal 0˚ crack orientation. Increasing crack width produces distinguishable variations in several resonant modes, particularly in the intermediate-frequency region. The changes arise because the horizontal crack intersects the electromagnetic-field distribution associated with the LV-shaped resonator and modifies the local effective permittivity beneath the sensing structure.

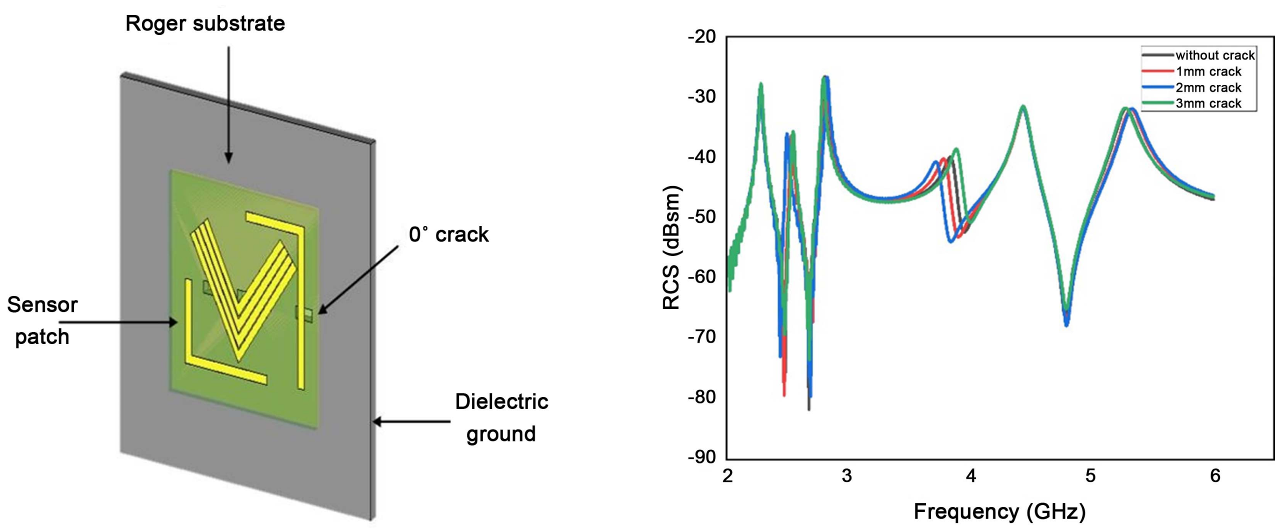

Figure 6. Multiresonance chipless RFID sensor tag placed on the dielectric material with varying crack orientations and crack widths at 0˚.

The individual resonances do not exhibit identical responses. Some modes undergo more noticeable frequency displacement, while others primarily show changes in peak amplitude or spectral prominence. This mode-dependent behavior indicates that the sensitivity of the proposed sensor is governed by the spatial overlap between the crack and the electromagnetic field associated with each resonant path. The combination of these resonance variations provides a characteristic spectral response for the 0˚ orientation.

Figure 7 shows the simulated RCS response for the vertical 90˚ crack orientation. Rotation of the crack from 0˚ to 90˚ changes its alignment relative to the dominant electric-field and surface-current paths. Consequently, the resulting resonance-shift pattern differs from that observed for the horizontal crack.

As the crack width increases, several resonant modes exhibit measurable frequency and amplitude variations. However, the variation is not uniformly linear across all widths and resonances. In particular, some modes display non-monotonic behavior, indicating that a single sensitivity coefficient cannot adequately represent the entire 90˚ response. These localized reversals may result from redistribution of the electromagnetic fields and changes in coupling between neighbouring resonant sections. Nevertheless, the collective multiresonance signature remains distinguishable from the responses obtained for the other crack orientations.

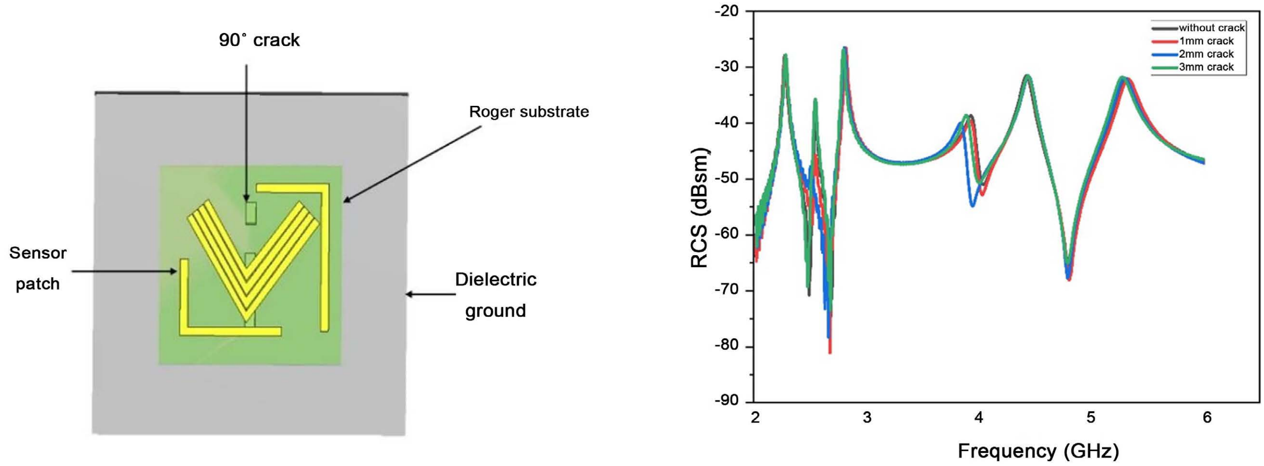

Figure 7. Multiresonance chipless RFID sensor tag placed on the dielectric square shape crack material with varying crack orientations and crack widths at 90˚.

Figure 8 illustrates the simulated RCS response for a 45˚ diagonal crack. Unlike the horizontal and vertical cases, the diagonal crack intersects multiple electromagnetic-field regions associated with both the L-shaped and V-shaped resonant

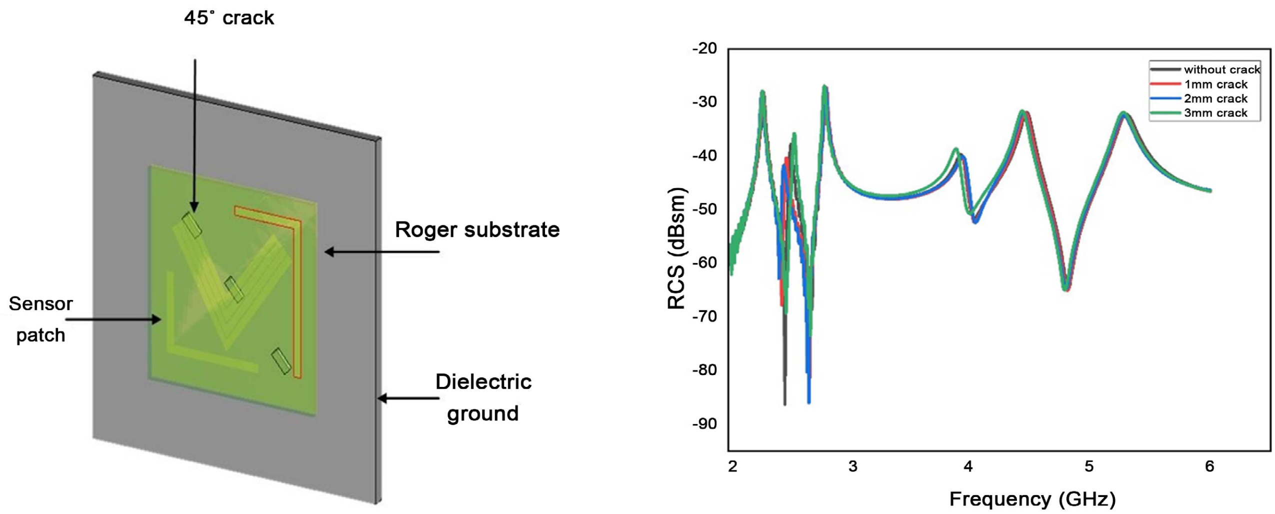

Figure 8. Multiresonance chipless RFID sensor tag placed on the dielectric square shape crack material with varying crack orientations and crack widths at 45˚.

elements. This asymmetric interaction produces mode-dependent spectral perturbations. The spectra show that different resonant modes respond differently as crack width increases. Certain resonances exhibit greater frequency displacement, whereas others show comparatively small changes or predominantly amplitude variations. The resulting mixed response demonstrates that crack orientation cannot be determined reliably from the direction of a single resonance shift. Instead, the relative variations of multiple resonant frequencies must be considered together to form an orientation-specific signature.

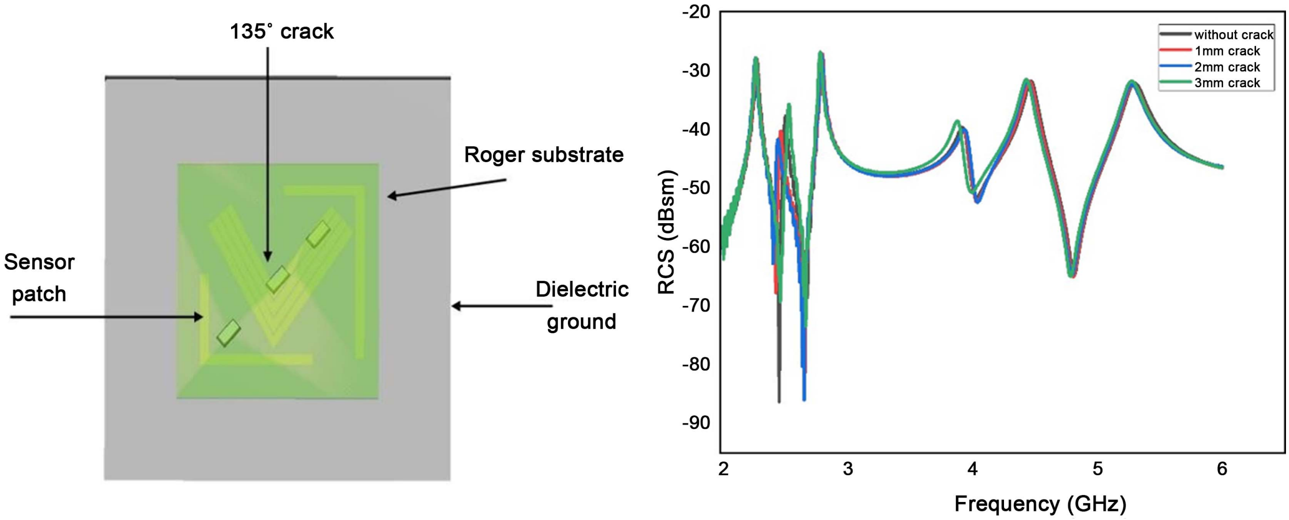

Figure 9. Multiresonance chipless RFID sensor tag placed on the dielectric square shape crack material with varying crack orientations and crack widths at 135˚.

Figure 9 presents the simulated RCS response of the proposed sensor for a 135˚ crack orientation with crack widths of 1, 2, and 3 mm, together with the intact reference condition. The overall multiresonance profile remains preserved across the 2 - 6 GHz band, while individual resonant modes exhibit different levels of frequency and amplitude variation as the crack width increases. The most visible changes occur mainly in the resonance region around 3.8 - 4.1 GHz, whereas the higher-frequency resonances show comparatively smaller but still distinguishable perturbations.

The 135˚ crack intersects the localized electromagnetic-field distribution in a direction different from the 45˚ case. Because the LV-shaped resonator is geometrically asymmetric, these two diagonal orientations do not produce identical electromagnetic loading. The 135˚ crack therefore perturbs a different combination of L-shaped and V-shaped current paths, resulting in an orientation-specific resonance pattern.

For smaller crack widths, the simulated curves remain relatively close to the intact response for several resonant modes, indicating limited dielectric perturbation within some sensing regions. As the crack width increases, the difference between the crack-loaded and intact responses becomes more visible, particularly for the resonances that exhibit stronger field interaction with the diagonal defect. This behavior indicates that the sensitivity of the sensor is mode-dependent and that not every resonance contributes equally to crack-width estimation.

The response in Figure 9 should therefore be interpreted using the collective multiresonance signature rather than by assuming a uniform upward or downward shift of all resonances. The relative frequency displacement, amplitude variation, and spectral separation of the selected modes together provide the characteristic signature of the 135˚ rack orientation. This combined response enables discrimination from the 0˚, 45˚, and 90˚ cases, provided that the same resonant modes are tracked consistently for all crack widths.

4.5. Quantitative Sensitivity and Linearity Assessment

The quantitative sensitivity of the proposed sensor was evaluated by tracking five consistently identifiable resonant features in the simulated radar cross-section spectra for crack widths of 1, 2, and 3 mm. The datasets for each crack orientation were generated using the same 2 - 6 GHz frequency range, RCS output definition, and 0.004 GHz frequency sampling interval, allowing direct comparison of the resonance-frequency variations.

To reduce the effect of the discrete frequency step, each resonance frequency was refined using local quadratic interpolation around the corresponding RCS extremum. Ordinary least-squares linear regression was then applied independently to each resonant mode according to

$$f_{i,\theta}(w) = S_{i,\theta} w + b_{i,\theta},$$

Table 2. Orientation-Dependent frequency sensitivity and linearity of the selected resonant modes.

Crack orientation	Mode	Frequency region (GHz)	Sensitivity (MHz/mm)	R2	Response behaviour
0˚	M1	2.33	−0.223	0.599	Weak variation
0˚	M2	2.72 - 2.73	−2.470	0.599	Non-monotonic
0˚	M3	3.94 - 3.96	−2.202	0.056	Non-monotonic
0˚	M4	4.51 - 4.52	−0.570	0.056	Non-monotonic
0˚	M5	5.14 - 5.17	−4.854	0.063	Non-monotonic
Orthogonal	M1	2.33	+0.788	0.832	Moderately linear
Orthogonal	M2	2.70 - 2.71	+0.975	0.521	Weak-to-moderate linearity
Orthogonal	M3	3.93	−1.223	0.995	Strong linear response
Orthogonal	M4	4.51	+0.117	0.021	Negligible/non-monotonic
Orthogonal	M5	5.11 - 5.12	+1.317	0.329	Poor linearity

Table 2 summarizes the orientation-dependent frequency sensitivity and linearity (R^2) of the selected resonant modes, providing a quantitative basis for identifying the most reliable modes for crack-width estimation.

For the 0˚ crack orientation, the tracked resonance frequencies do not exhibit a consistently monotonic relationship with crack width. Although numerical slopes can be obtained from linear regression, the corresponding coefficients of determination are low, with R^2 values ranging from 0.056 to 0.599. Therefore, these modes should not be interpreted as reliable linear crack-width indicators. Instead, their combined frequency and amplitude variations may be used as supplementary spectral features for distinguishing crack orientation and severity. The three datasets used for the 0˚ analysis correspond to crack widths of 1, 2, and 3 mm and share the same CST simulation format and frequency sampling.

For the orthogonal crack orientation, the resonance located near 3.93 GHz shows the strongest and most consistent dependence on crack width. The resonance frequency decreases from approximately 3.932 GHz at a crack width of 1 mm to approximately 3.930 GHz at 2 mm and 3.929 GHz at 3 mm. The corresponding linear regression gives

$$f(w) = -0.001223w + 3.933088 \text{ GHz},$$

with a sensitivity of

$$S = -1.223 \text{ MHz/mm}$$

and a coefficient of determination of

$$R^2 = 0.995.$$

This high R^2 value indicates that the frequency shift of this mode is approximately linear over the investigated crack-width range. Consequently, the resonance near 3.93 GHz may be used as the primary quantitative feature for estimating crack width under the orthogonal orientation.

The resonance near 2.33 GHz also exhibits a moderately consistent response, with a positive sensitivity of 0.788 MHz/mm and $R^2 = 0.832$. However, its linearity is lower than that of the 3.93 GHz mode. The remaining orthogonal modes exhibit either weak or non-monotonic frequency changes and are therefore more suitable as complementary classification features rather than independent crack-width estimators. The orthogonal datasets were also obtained for crack widths of 1, 2, and 3 mm under identical frequency-sweep and RCS-output settings.

Overall, the results demonstrate that the crack-sensing response is both mode-dependent and orientation-dependent. A uniform upward or downward shift cannot be assumed for all resonances. Instead, selected resonant modes with high linearity should be used for quantitative crack-width estimation, while the complete multiresonance signature can be employed for crack-orientation discrimination. It should also be noted that the regression analysis is based on three simulated crack-width cases. Therefore, the reported sensitivity represents the response over the investigated range of 1 - 3 mm and should not be extrapolated beyond this range without additional simulations or experimental validation.

4.6. Crack Width and Orientation Estimation

The proposed sensing methodology estimates crack characteristics by comparing the measured multiresonance RCS spectrum with the reference spectrum of the intact structure. For each resonant mode, the resonance frequency is extracted from the measured RCS response, and the corresponding frequency shift is calculated as

$$\Delta f_i = f_i - f_{i,0}, \tag{1.9}$$

where $f_{i,0}$ is the resonance frequency of the intact sensor and f_i is the measured resonance frequency after crack formation.

For resonant modes exhibiting an approximately linear response, the crack width can be estimated using the regression model

$$w = \frac{f_i - b_i}{S_i}, \tag{1.10}$$

where S_i is the sensitivity obtained from the linear regression analysis and b_i is the corresponding regression intercept.

Rather than relying on a single resonance, the proposed sensor exploits the complete multiresonance signature. Different crack orientations perturb different resonant modes because the crack interacts differently with the current distribution of the asymmetric LV resonators. Consequently, the collective frequency-shift pattern provides orientation-dependent information, while the most linear resonant modes can be used for quantitative crack-width estimation.

5. Proposed Reader Configuration and Simulated Interrogation Framework

The proposed chipless RFID sensing system is illustrated using a conceptual interrogation framework operating over the 2 - 6 GHz frequency range. The framework consists of two broadband antipodal Vivaldi antennas arranged in a cross-polarized configuration, where one antenna transmits the incident electromagnetic wave and the second antenna receives the backscattered response from the sensing tag. This configuration is presented to demonstrate a practical implementation of the proposed sensing concept and to illustrate how the tag may be interrogated in a real measurement environment.

As shown in **Figure 10**, the sensing tag is positioned on the dielectric specimen containing the crack defect. Variations in crack width and orientation modify the electromagnetic interaction between the resonator and the surrounding dielectric material, resulting in changes in the resonance frequencies of the scattered RCS spectrum. These resonance-frequency variations constitute the sensing signature used for crack characterization.

It should be emphasized that the reader configuration shown in **Figure 10** was not explicitly modelled or experimentally implemented in this work. All resonance characteristics, frequency shifts, sensitivity values, and crack-characterization results presented in this paper were obtained exclusively from full-wave electromagnetic simulations performed in CST Studio Suite. The reported spectra therefore represent simulated monostatic radar cross-section (RCS) responses of the proposed chipless RFID sensor rather than signals acquired from a physical interrogation system.

In a practical implementation, the backscattered response could be measured using broadband antennas and conventional RF instrumentation, followed by resonance extraction using standard peak-detection or curve-fitting techniques. The design and experimental validation of such a hardware interrogation system are beyond the scope of the present work and will be considered in future studies.

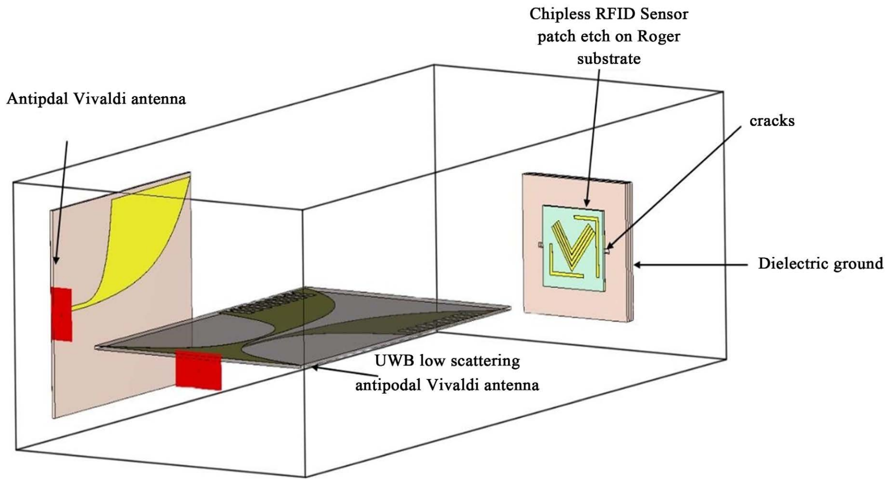

Figure 10. Chipless RFID sensor with UWB low scattering and antipodal Vivaldi antenna (AVA).

The reader antennas are arranged in an orthogonal configuration to optimize polarization diversity and improve the robustness of backscatter detection. Specifically, the ultra-wideband (UWB) low-scattering antipodal Vivaldi antenna is oriented vertically, while the antipodal Vivaldi antenna (AVA) is positioned horizontally. This cross-oriented arrangement enhances isolation between transmitted and received signals, thereby improving the accuracy of chipless RFID tag interrogation.

To compensate for the inherently low backscattered power of chipless RFID tags, high-gain antennas are employed at the reader side, with gain values ranging from 7 dBi to 10.2 dBi across the 2 - 6 GHz operating band. This ensures sufficient link budget for reliable detection of weak multiresonance responses from the sensor tag under practical conditions.

The simulated RCS spectra obtained from CST Studio Suite were analyzed to evaluate crack-induced resonance variations. The six resonant modes shown in Figure 11 and Figure 12 constitute the sensing features used for crack characterization. The spectral response exhibits six distinct resonance peaks corresponding to the designed LV-shaped resonator structure.

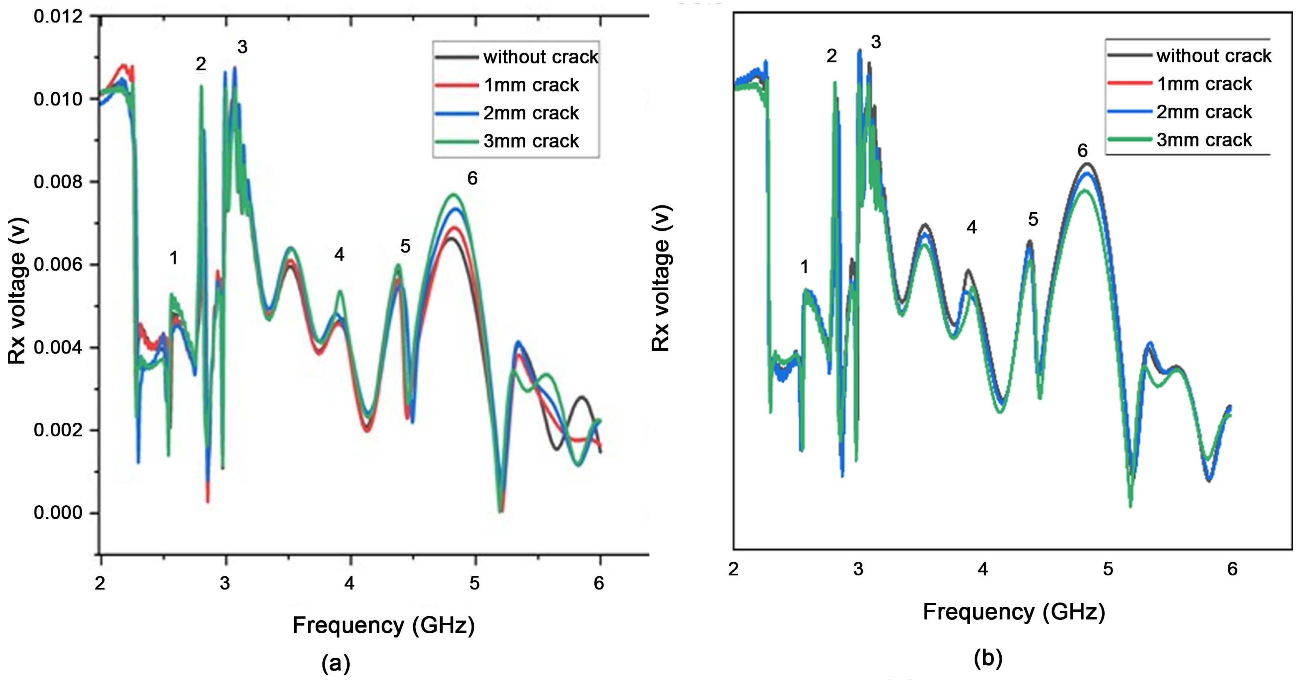

Figure 11. The multiresonance chipless RFID sensor tag attached to the crack with varying crack orientations and crack widths: (a) at; (b) at.

Figure 11(a) illustrates the simulated multiresonance spectral response of the proposed chipless RFID sensor for dielectric cracks oriented at 0˚ with different crack widths. As the crack width increases, the electromagnetic coupling between the LV-shaped resonator and the polyamide substrate is progressively modified due to the reduction in the effective dielectric loading within the sensing region. This perturbation results in measurable variations in the resonance spectrum, where several resonant modes exhibit frequency shifts with different sensitivities. The response demonstrates that the proposed sensor can distinguish different crack widths while maintaining a stable multiresonance signature throughout the operating bandwidth. The observed resonance variations indicate that crack width directly influences the electromagnetic field distribution around the resonator, thereby providing a reliable indicator for structural defect characterization.

Figure 11(b) presents the simulated resonance response for 45˚ crack orientation. Compared with the 0˚ orientation, the resonant signatures exhibit a different frequency-shift pattern because the crack intersects the localized electric-field distribution at a different angle. Consequently, the electromagnetic interaction between the resonator and the dielectric material changes, resulting in orientation-dependent resonance behavior. Although the overall multiresonance characteristics are preserved, the relative sensitivity of individual resonances differs from that observed in **Figure 11(a)**, demonstrating that the sensor is capable of discriminating crack orientation in addition to crack width.

Figure 12(a) shows the simulated resonance spectra for 90˚ crack orientation under different crack widths. Similar to the previous cases, increasing crack width modifies the effective dielectric environment surrounding the resonator, producing systematic perturbations in the resonance frequencies. The resulting spectral response remains clearly distinguishable for each crack condition, confirming that the proposed multiresonance sensor maintains consistent sensing capability irrespective of crack orientation. The differences in resonance behavior relative to Figure 11(a) and Figure 11(b) further indicate that the orientation of the crack significantly influences the electromagnetic coupling mechanism and consequently the resonance signature.

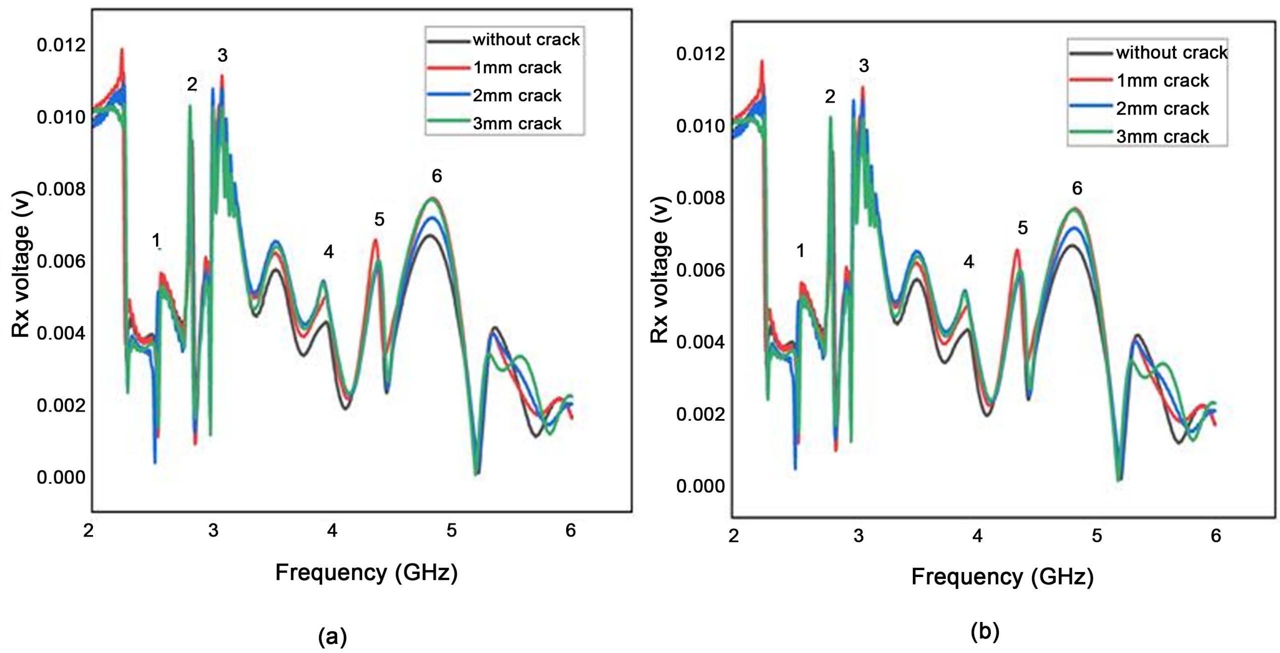

Figure 12. The multiresonance chipless RFID sensor tag attached to the crack samples with varying crack orientations and crack widths: (a) at; (b) at.

Figure 12(b) illustrates the spectral response for 135˚ crack orientation. The resonance characteristics continue to exhibit orientation-dependent behavior, with several resonant modes showing distinguishable frequency variations as the crack width increases. These variations arise from changes in the distribution of the electric fields around the resonator caused by the altered crack geometry. The unique resonance signature associated with this orientation further demonstrates the capability of the proposed chipless RFID sensor to identify multiple crack configurations using a single passive sensing structure.

Overall, Figure 11 and Figure 12 demonstrate that the proposed multiresonance chipless RFID sensor produces distinct and repeatable resonance signatures for different combinations of crack width and orientation. Rather than relying on a single resonant frequency, the sensor exploits the collective response of multiple resonant modes, thereby improving defect discrimination and enhancing sensing reliability. Since each crack orientation produces a unique resonance pattern, the multiresonance response provides sufficient information to characterize both the severity and orientation of dielectric cracks. All resonance spectra presented in Figure 11 and Figure 12 were obtained from full-wave electromagnetic simulations using CST Studio Suite and represent the simulated backscattered response of the proposed interrogation framework. No experimental measurements, receiver-voltage acquisition, or hardware signal-processing implementation were performed in this study.

Table 3. Comparison on proposed work and previous studies related to chipless RFID sensor designs for crack detection.

Study/Work	Method Used	Defect/Parameter Measured	Frequency Range	Results/Observations	Limitations
Our work	Multi-resonance chipless RFID sensor with LV-shaped patches and UWB Antipodal Vivaldi antenna for far field chipless RFID	Crack size and orientation	2.3 GHz to 5 GHz	Distinct resonance-frequency shifts observed across various crack sizes (1 mm to 3 mm). High sensitivity for crack detection and precise resonance shifts in both metallic and dielectric surface.	Requires advanced signal processing for environmental noise, potential read range limitations in real-world conditions.
Marinda *et al.* (2018) [12]	Chipless RFID sensor tag with UWB frequency signature and dipole encoders for metal crack detection.	Crack detection in metal	2 - 6 GHz	High resolution for crack detection only in metallic surfaces.	Narrow read range (<1 m), metal dependency, and susceptibility to interference.
Amin *et al.* (2013) [5]	Spiral resonator-based chipless RFID sensor for humidity sensing.	Humidity	2.45 GHz	Low-cost and printable, sensitive to environmental changes in humidity.	Limited bit capacity, short read range, fragile in high-temperature environments...
Zhao *et al.* (2017) [8]	Miniaturized UHF RFID patch antenna sensor for corrosion characterization.	Corrosion on metal surfaces	2.4 - 2.485 GHz	Capable of detecting corrosion with standard UHF readers.	Uniform current distribution limits sensitivity, requires close proximity for accurate detection.
Karami-Horestani *et al.* (2023) [10]	Hybrid time/phase domain synchronous electromagnetic encoders for near-field chipless RFID.	Motion control and defect detection	UHF and MHz range	Capable of high-resolution motion control and defect detection.	Complex hardware, requires accurate synchronization, limited scalability for large structures.

Table 3 compares the proposed multiresonance chipless RFID sensor with representative prior sensor designs in terms of sensing method, measured parameter, operating frequency range, and reported advantages and limitations.

6. Comparative Analysis with Existing State-of-the-Art Methods

In comparison with existing state-of-the-art chipless RFID sensing approaches, the proposed multiresonance LV-shaped sensor demonstrates clear improvements in crack detection capability, operational robustness, and structural health monitoring functionality. Prior works such as [12] and [8] primarily focus on single-parameter sensing and are largely constrained to metallic surfaces, limiting their applicability in dielectric-based structural monitoring scenarios.

In contrast, the proposed design introduces a multiresonant LV-shaped architecture that enables simultaneous extraction of crack width and orientation through distinct frequency shift patterns. This significantly enhances the information-carrying capacity of the sensor compared to conventional single- or dual-resonance chipless RFID tags.

Compared to spiral resonator-based sensing techniques [5], which exhibit sensitivity to environmental variations such as humidity and suffer from limited resolution stability, the proposed system maintains consistent multiresonance behavior across a wide UWB operating band (2.3 - 5 GHz). This results in improved frequency stability, higher encoding reliability, and enhanced defect discrimination capability.

Furthermore, the integration of a UWB antipodal Vivaldi antenna improves radiation efficiency and bandwidth performance compared to narrowband reader architectures commonly reported in earlier studies. The proposed system also benefits from passive operation, low cost, and scalable deployment, while calibration-based signal processing effectively mitigates noise and false peak detection issues.

Overall, the proposed chipless RFID sensor overcomes key limitations of existing approaches, including substrate dependency, limited read range, and single-parameter sensing, thereby providing a more robust and adaptable solution for dielectric crack monitoring in structural health monitoring applications.

7. Conclusions

This study presented the design and analysis of a wideband multiresonance chipless RFID sensor for the detection and characterization of dielectric cracks in structural materials. The proposed LV-shaped resonator architecture demonstrates that key crack parameters, including width and orientation, can be effectively extracted through distinct multiresonance frequency shift patterns.

The results confirm that the developed sensing framework, combined with cross-polarization interrogation and an antipodal Vivaldi antenna-based reader, enables reliable detection of defect-induced variations in the frequency signature.

The proposed system successfully characterizes crack orientations of 0˚, 45˚, 90˚, and 135˚, as well as crack widths ranging from 1 mm to 3 mm.

A depolarizing chipless RFID tag configuration, together with controlled near-field interrogation at a fixed reading distance of approximately 15 cm, ensures stable extraction of the multiresonance spectral response even in the presence of a large monitored dielectric structure. The use of cross-polarized measurement further enhances signal isolation and improves detection robustness.

Overall, the proposed LV-shaped multiresonance chipless RFID sensor provides a compact, passive, and high-resolution sensing solution with strong radar cross-section performance. Compared with conventional chipless RFID approaches, it offers improved feature richness, enhanced defect discrimination capability, and better suitability for practical structural health monitoring applications.

The presented approach demonstrates strong potential for future deployment in infrastructure monitoring systems, where low-cost, scalable, and wireless non-destructive evaluation techniques are required. Future work may focus on extending read range, improving multi-tag discrimination, and experimental validation in real-world environments.

8. Future Work and Perspectives

The results presented in this study highlight the strong potential of the proposed chipless RFID-based sensing system for structural health monitoring of critical infrastructure, including railways, pipelines, and oil storage tanks. Despite these promising outcomes, several practical challenges must be addressed to enable large-scale field deployment and system integration.

A key limitation lies in improving the maximum reading range and overall detection accuracy. Future design optimization should focus on identifying an optimal tag topology that balances spectral encoding capacity, spatial resolution, and interrogation distance. Although miniaturization of chipless RFID tags remains an active research direction, it presents significant challenges due to inherent trade-offs between size reduction and resonance stability.

Further research is also required to overcome current technological constraints and to expand the application scope of passive multiresonance chipless RFID sensors. Future developments can be broadly categorized into three main directions.

1) **Networking and standardization:** development of tag arrays and controlled tag-tag coupling mechanisms for improved coverage, along with integration of ultra-wideband (UWB) techniques for high-capacity data encoding and robust interrogation.

2) **Flexibility and ubiquity:** integration with hybrid sensing platforms combining chipless RFID with embedded sensor technologies, implementation of automated impedance matching and digital RSSI processing, exploration of functional materials for analog memory behavior, and adaptation for wearable and biomed-

ical sensing applications.

Overall, these directions indicate a pathway toward more intelligent, scalable, and multifunctional chipless RFID systems for next-generation structural health monitoring and sensing networks.

Acknowledgements

The authors would like to express their sincere appreciation to the School of Information and Communication Engineering, Northwestern Polytechnical University, for providing academic and research support during the development of this work. The authors also gratefully acknowledge the valuable technical discussions and suggestions received during the preparation of this manuscript.

Author Contributions

Conceptualization, M.Z.; methodology, M.Z.; software and simulation, M.Z.; formal analysis, M.Z.; investigation, M.Z.; data curation, M.Z.; visualization, M.Z.; writing—original draft preparation, M.Z.; writing—review and editing, F.Z.K., M.K.S. and A.G.A.; supervision and technical guidance, F.Z.K., M.K.S. and A.G.A. All authors have read and agreed to the published version of the manuscript.

Conflicts of Interest

The authors declare no conflicts of interest regarding the publication of this paper.

References

[1] Avci, O., Abdeljaber, O., Kiranyaz, S., Hussein, M., Gabbouj, M. and Inman, D.J. (2021) A Review of Vibration-Based Damage Detection in Civil Structures: From Traditional Methods to Machine Learning and Deep Learning Applications. *Mechanical Systems and Signal Processing*, **147**, Article ID: 107077. https://doi.org/10.1016/j.ymssp.2020.107077

[2] Vagnoli, M., Remenyte-Prescott, R. and Andrews, J. (2017) Railway Bridge Structural Health Monitoring and Fault Detection: State-of-the-Art Methods and Future Challenges. *Structural Health Monitoring*, **17**, 971-1007. https://doi.org/10.1177/1475921717721137

[3] Ling, J.T., Feng, K., Wang, T., Liao, M., Yang, C.S. and Liu, Z. (2023) Data Modeling Techniques for Pipeline Integrity Assessment: A State-of-the-Art Survey. *IEEE Transactions on Instrumentation and Measurement*, **72**, 1-17. https://doi.org/10.1109/tim.2023.3279910

[4] Wang, B., Zhong, S., Lee, T.L., Fancey, K.S. and Mi, J. (2020) Non-Destructive Testing and Evaluation of Composite Materials/Structures: A State-of-the-Art Review. *Advances in Mechanical Engineering*, **12**. https://doi.org/10.1177/1687814020913761

[5] Amin, E.M., Bhuiyan, M.S., Karmakar, N.C. and Winther-Jensen, B. (2014) Development of a Low Cost Printable Chipless RFID Humidity Sensor. *IEEE Sensors Journal*, **14**, 140-149. https://doi.org/10.1109/jsen.2013.2278560

[6] Zahid, M.N., Gaofeng, Z., Sadiq, T., Rahman, H. and Anwar, M.S. (2024) A Comprehensive Study of Chipless RFID Sensors for Healthcare Applications. *IEEE Access*,

12, 175647-175665. https://doi.org/10.1109/access.2024.3446994

[7] Suneel Kumar, C. and Patre, S.R. (2025) Passive Chipless RFID Tags for Humidity Sensing: A Review. *IEEE Journal of Radio Frequency Identification*, **9**, 200-214. https://doi.org/10.1109/jrfid.2025.3562719

[8] Zhao, A., Zhang, J. and Tian, G.Y. (2017) Miniaturization of UHF RFID Tag Antenna Sensors for Corrosion Characterization. *IEEE Sensors Journal*, **17**, 7908-7916. https://doi.org/10.1109/jsen.2017.2751587

[9] Salmerón, J.F., Rivadeneyra, A., Agudo-Acemel, M., Capitán-Vallvey, L.F., Banqueri, J., Carvajal, M.A., *et al.* (2014) Printed Single-Chip UHF Passive Radio Frequency Identification Tags with Sensing Capability. *Sensors and Actuators A*: *Physical*, **220**, 281-289. https://doi.org/10.1016/j.sna.2014.10.023

[10] Karami-Horestani, A., Paredes, F. and Martín, F. (2023) Hybrid Time/Phase Domain Synchronous Electromagnetic Encoders for Near-Field Chipless-RFID and Motion Control Applications. *IEEE Transactions on Microwave Theory and Techniques*, **71**, 5457-5469. https://doi.org/10.1109/tmtt.2023.3277934

[11] Xie, Y.M., Hu, J.W., Yang, Y.L., Wan, G.C. and Xie, L.Y. (2023) A Novel 4-Bit U-Shaped Chipless Flexible Substrate RFID Sensor Sensing Characterization Study. *IEEE Access*, **11**, 128655-128666. https://doi.org/10.1109/access.2023.3333048

[12] Marindra, A.M.J. and Tian, G.Y. (2018) Chipless RFID Sensor Tag for Metal Crack Detection and Characterization. *IEEE Transactions on Microwave Theory and Techniques*, **66**, 2452-2462. https://doi.org/10.1109/tmtt.2017.2786696

[13] Dey, S., Kalansuriya, P. and Karmakar, N.C. (2021) Novel Chipless RFID High Resolution Crack Sensor Based on SWB Technology. *IEEE Sensors Journal*, **21**, 2908-2920. https://doi.org/10.1109/jsen.2020.3028296

[14] Zhang, M., Li, M., Xu, W., Zhang, F., Yao, D., Wang, X., *et al.* (2024) Soft Wireless Passive Chipless Sensors for Biological Applications: A Review. *Biosensors*, **15**, Article 6. https://doi.org/10.3390/bios15010006

[15] Mishra, D.P. and Behera, S.K. (2023) Resonator Based Chipless RFID: A Frequency Domain Comprehensive Review. *IEEE Transactions on Instrumentation and Measurement*, **72**, 1-16. https://doi.org/10.1109/tim.2022.3225027

[16] Vena, A., Perret, E. and Tedjni, S. (2013) A Depolarizing Chipless RFID Tag for Robust Detection and Its FCC Compliant UWB Reading System. *IEEE Transactions on Microwave Theory and Techniques*, **61**, 2982-2994. https://doi.org/10.1109/tmtt.2013.2267748

[17] Costa, F., Genovesi, S. and Monorchio, A. (2014) Reading Chipless RFID Located on Metallic Platforms by Using Cross-Polar Scattering. 2014 *XXXIth URSI General Assembly and Scientific Symposium* (*URSI GASS*), Beijing, 16-23 August 2014, 1-4. https://doi.org/10.1109/ursigass.2014.6929188

[18] Volakis, J.L. and Volakis, J.L. (2007) Antenna Engineering Handbook. McGraw-Hill.

[19] Gotoh, Y., Hirano, H., Nakano, M., Fujiwara, K. and Takahashi, N. (2005) Electromagnetic Nondestructive Testing of Rust Region in Steel. *IEEE Transactions on Magnetics*, **41**, 3616-3618. https://doi.org/10.1109/tmag.2005.855174

[20] Karmaker, N.C. (2016) Tag, You're It Radar Cross Section of Chipless RFID Tags. *IEEE Microwave Magazine*, **17**, 64-74. https://doi.org/10.1109/mmm.2016.2549160

[21] Karmakar, N.C., Kalansuriya, P., Azim, R.E. and Koswatta, R. (2016) Chipless Radio Frequency Identification Reader Signal Processing. Wiley. https://doi.org/10.1002/9781119215783

[22] Rance, O., Perret, E., Siragusa, R. and Lemaître-Auger, P. (2017) RCS Synthesis for Chipless RFID: Theory and Design. Elsevier.

[23] Vena, A., Perret, E. and Tedjini, S. (2016) Chipless RFID Based on RF Encoding Particle: Realization, Coding and Reading System. Elsevier.

Supplementary Work

Cracks in Dielectric Material

Crack and corrosion are two kinds of defects that have been identified as causes of structural failures in the dielectric material. Repeated application of weights and exposure to harsh environmental conditions can cause crack and corrosion, affecting the integrity of dielectric structures. The degradation can start in the form of minor defects, become more noticeable over time, and finally lead to catastrophic failures. Crack and corrosion are two distinct phenomena, but they both represent severe threats to infrastructure safety. This section examines the crack and corrosion mechanisms in dielectric structures, their fundamental properties, and the challenges they pose related to sensing. The described system is based on identifying the cracks on different materials before the work has been done on simple metals such as steel, aluminum, etc. Our work is based on the detection of cracks in dielectric materials. Cracks are the most frequent and harmful for any materials such (as steel, aluminum, etc.) because they diminish the cross-section of a structure, hence reducing its structural capability. In addition to mechanical stress, such as fatigue, structures may develop cracks because of various physical and chemical processes (stress corrosion). Strain and corrosion can also be monitored using multiresonance chipless RFID sensor systems, enabling early detection of structural health problems. The crack's width varies from 1 mm to 3 mm, but the length and depth of the crack is fixed. Cracks can occur at different orientations; Figure S1 illustrates the representative crack orientations from 0˚ to 135˚ considered for the dielectric material.

As shown in Figure S1, the dielectric crack model includes multiple representative orientations, enabling evaluation of orientation-dependent changes in the multiresonance response.

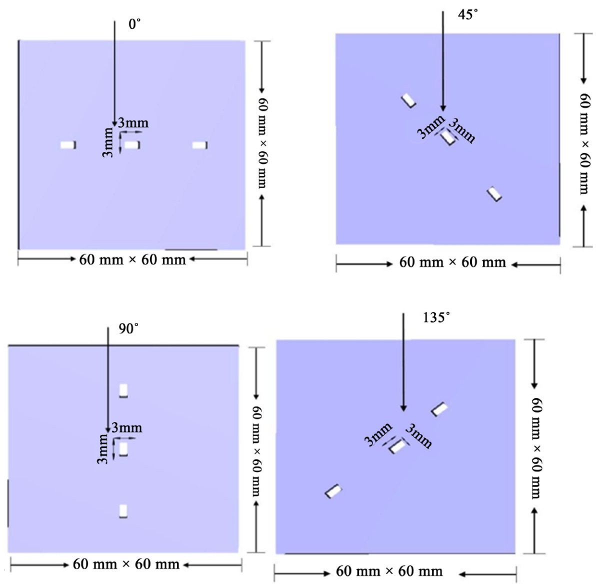

Figure S1. Different cracks orientation in the dielectric material.